# Generation and propagation of coherent phonon beams

E. P. N. Damen, D. J. Dieleman, A. F. M. Arts, and H. W. de Wijn
*Faculty of Physics and Astronomy, and Debye Institute, Utrecht University, P.O. Box 80.000, 3508 TA Utrecht, The Netherlands*
(Received 2 January 2001; revised manuscript received 21 May 2001; published 5 October 2001)

Narrow coherent beams of longitudinal acoustic waves are injected into a single crystal of $PbMoO_4$ at gigahertz frequencies, and their properties are observed by means of Brillouin scattering. The waves are generated via the thermoelastic strain that results from periodic surface heating of a thin metallic transducer by interfering cw dye lasers. Frequency tuning is achieved simply by varying the optical difference frequency. A theoretical description based on heat diffusion and thermoelastic expansion agrees with the observed frequency dependence of the acoustic intensity, inclusive of acoustic resonances within the transducer, as well as its quadratic dependence on the laser power. The propagation of the acoustic beams is found to be governed by Fresnel diffraction provided due account is taken of phonon focusing. The beam furthermore is responsive to the phase profile over the laser-illuminated area, which allows us to manipulate the beam in various ways, such as modifying its divergence as if an acoustic lens were positioned just below the transducer or sweeping the beam sideward by a moving grating. Combined with Brillouin detection, distinguishing between phase and group velocities, this provides a direct measurement of phonon focusing. Finally, the decay of the acoustic beam with the distance is measured at various frequencies, to find confirmation of Herring's asymptotic theory for anharmonic phonon decay in anisotropic crystals.

DOI: 10.1103/PhysRevB.64.174303 PACS number(s): 63.20.−e

## I. INTRODUCTION

In this paper we report on the generation and propagation of narrow Fresnel-diffracted coherent phonon beams. The beams are generated by periodic laser-induced thermomodulation of a thin metallic transducer. Following injection into a single-crystalline material, they are detected at some distance by Brillouin scattering, to observe their divergence due to their finite wavelength, their decay by anharmonicity, and their direction of propagation as it depends on phonon focusing and the phase distribution in the ''orifice'' of generation. Purely harmonic surface heating is particularly attractive, because it generates a coherent wave synchronous with the modulated heat, as was first pointed out by White.[1] The realization of this notion has however been little successful in comparison with the achievements of phonon sources delivering a Planckian spectrum or a spectrum of limited width, notably heat pulses,[2] superconducting tunnel junctions,[3,4] and optical techniques.[5] The unfortunate fact is that the acoustic intensity is quadratic in the heating power and, accordingly, very low for the power densities available from conventional oscillatory heating. Pulsed thermoelastic expansion, such as by heating with a high-power picosecond pulsed laser,[6] has on the other hand won its spurs in the time domain.

The work has been motivated by the desire to have a tunable source delivering a narrow coherent beam of phonons in the gigahertz range.[7] Not only makes such a source true phonon spectroscopy possible, but it also brings within reach ''physical optics'' of phonons, such as diffraction, and the frequency-resolved measurement of phonon decay. The heating, achieved by two interfering single-frequency lasers operating at slightly different frequencies, is sinusoidal, continuous, and of negligible spectral width, but enhanced to workable proportions by focusing the optical energy onto a tiny spot. At gigahertz frequencies and beyond, only good conductors can be effective as phonon generator by thermomodulation, because the energy need be absorbed within a distance shorter than the acoustic wavelength. A thin metallic transducer is therefore used to convert the laser-induced heating into the strain wave that is injected into the specimen.

Section II provides experimental details concerning the laser-induced heating and the detection by Brillouin scattering. Section III focuses on the thermoinduced generation mechanism as such, i.e., an acoustic wave which via thermal expansion is driven by oscillatory heat diffusing into a thin metallic transducer. Resonant standing waves within the transducer, much like in interferometers, enhance the strain injected into the crystal. Section IV deals with the acoustic beam as it propagates through the crystal. The beam is found to be Fresnel diffracted with a divergence on the order of a few degrees of arc. In a more precise treatment, the divergence is shown to bear the effects of phonon focusing[8–10] as well as nonuniformity in the phase profile of the laser heating. This phase profile may be static and accountable by an acoustic lens or dynamic in the form of sideward moving grating, resulting in the acoustic beam being swept aside in consistency with phonon focusing. Section IV finally shows that the beam is excellently suited to measure phonon decay as a function of the frequency.

## II. EXPERIMENTAL DETAILS

Two cw actively stabilized single-frequency ring dye lasers (Coherent 599 and 699) are used to produce thermomodulation in an approximately 500-nm-thick gold transducer deposited onto the single-crystalline specimen. The dye lasers are pumped by a single 15-W argon-ion laser and operate with Rhodamine 6G dye. Each of them delivers typically 500 mW of light in the $TEM_{00}$ mode at a wavelength of approximately 580 nm, with an essentially cylindrical Gauss-

 

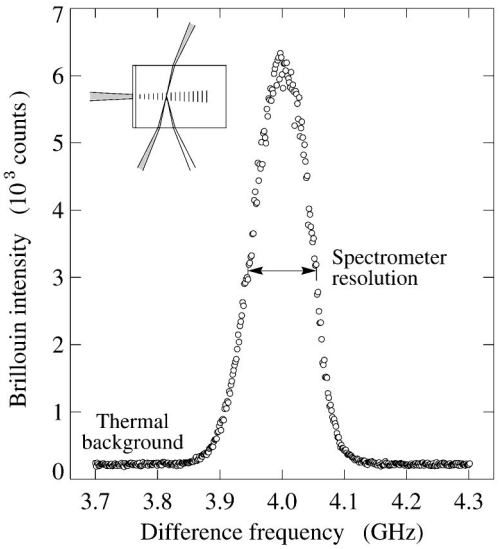


FIG. 1. The Brillouin intensity vs the frequency difference between the two ring dye lasers. The intensity is maximum at 4.00 GHz, where the optical difference frequency best matches the Bragg condition. The spread in the Brillouin condition is $\pm 0.055$ GHz at half maximum. The dwell time per data point is 200 ms. The thermal background is about 200 counts. The inset shows the principle of the experiment.

ian intensity distribution. A wave meter (Burleigh WA-20VIS), an optical spectrum analyzer, and the beat voltage produced over a fast photodiode monitor the dye-laser frequencies with increasing frequency resolution and decreasing frequency span. The desired phonon frequency of a few gigahertz, matching the frequency difference of the dye lasers, was thus found to be maintained to within 60 MHz over periods of several hours. More importantly, coherence among the two lasers appears to be preserved over times as long as 300 ns, i.e., a short-term spectral purity of order 1 MHz, which corresponds to a coherence length of several millimeters for the generated acoustic waves. The two dye-laser beams are aligned to coincidence and subsequently focused onto the transducer by a single lens to form an intensely illuminated spot, approximately 40 $\mu$m in diameter and intensity modulated to a depth of typically 80%. Usually the free face of the transducer is illuminated, but effective phonon generation may also be achieved by thermomodulation of the side facing the crystal. The thermomodulated transducer in turn injects a monochromatic strain wave into the crystal with a cross section equal to the focal area.

For the detection of the acoustic intensity we rely on Brillouin spectroscopy, because of its preeminent selectivity for wave vector, frequency, and location. The propagating acoustic wave reflects a small fraction of a narrow light beam, delivered by a separate single-mode argon-ion laser producing 200 mW of light at a wavelength of 514.5 nm (inset to Fig. 1). The light frequency is shifted upward or downward by the phonon frequency, while the phonon wave vector closes the wave vectors of the incident and scattered light. The detection volume is in the first instance narrowed down by focusing the Brillouin argon-laser beam to a pencil as thin as 10 $\mu$m in diameter. In length the detection volume is delimited to a typically 400-$\mu$m-long section of the pencil by the receiving optics, i.e., the *étendue* determined by the opening angle and active area of the interferometer. Note that the detection volume completely traverses the phonon beam, so that integration of the Brillouin intensity along the $x$ direction is implied.

The scattered light is analyzed with a quintuple-pass Fabry-Perot interferometer (Burleigh RC-110) acting as a fixed-frequency filter. The Fabry-Perot interferometer's transmission curve is actively optimized in finesse and locked to the center frequency of the anti-Stokes phonon line (Burleigh DAS-10). Its width typically is $\pm 0.055$ GHz at half maximum. The scattered light is subsequently passed through a low-resolution monochromator to suppress parasitic laser-plasma and Raman lines, and finally detected with a high-sensitivity photomultiplier followed by standard photon-counting and averaging techniques. At room temperature, therefore, the generated monochromatic phonons are observed on top of a background of thermal phonons satisfying the scattering condition. The photomultiplier, which is at the risk of overload by Rayleigh scattering, is protected by a fast electronic circuit limiting the anode current.[11]

The specimen is a cuboidal single crystal of lead molybdate ($PbMoO_4$), as mineral known as wulfenite. It was chosen for its transparency and its high acousto-optic constant [$M_2 = 50 \times 10^{-15}$ m$^2$/W (Ref. 12)], ensuring optimal Brillouin efficiency. $PbMoO_4$ has the tetragonal Scheelite structure (space group $C_{4h}^6$ or $I4_1/a$), with a four-molecule unit cell having edges $a_0 = 5.47$ Å and $c_0 = 12.18$ Å. It has mass density $\rho = 6.95$ g/cm$^3$, and is optically double refractive with refractive indices $n_o = 2.469$ (ordinary wave) and $n_e = 2.315$ (extraordinary wave) at 514.5 nm. The crystal, measuring $10 \times 11 \times 9$ mm$^3$ with finely polished faces, is cut such that the fourfold symmetric $c$ axis is parallel to the sides. The gold transducer, deposited onto a face perpendicular to the $c$ axis, is composed of four steps with thickness $d = 220$, 330, 440, and 660 nm. A thin 4-nm intermediate layer of chromium was applied for better adhesion to the crystal. The sample was held at room temperature, unless noted otherwise.

To demonstrate that thermomodulation generates an acoustic wave of a specific frequency, the anti-Stokes Brillouin intensity was measured versus the frequency difference of the dye lasers. In Fig. 1, the Brillouin condition was set for optimum detection of longitudinal 4.00-GHz phonons propagating along the $c$ axis. Indeed, a maximum in the intensity is observed at the point where the optical difference frequency matches the Brillouin condition. Figure 1 also makes us realize that the frequency spread of the signal relates to the resolving power of the Brillouin detection rather than the frequency spread of the generated acoustic beam ($\sim 1$ MHz). In Fig. 1 the peak intensity is 30 times the thermal background, but ratios of several hundreds have been observed, dependent on the frequency, the temperature, the specifications of the transducer, and, because of attenuation, the distance. This number is confirmed by an estimate based on Eq. (11) derived below in combination with the theoretical Brillouin-scattering cross section.[13] Self-

evidently, in all subsequent experiments the optical difference frequency and the location of the joint dye laser focus were tuned to maximum Brillouin response.

## III. THERMOMODULATION

We consider an energy flux $\Phi_0+\Phi_\omega \sin \omega t$ supplied to the free surface of a metallic transducer by interfering dye lasers of approximately equal intensity and operating at an angular optical difference frequency $\omega$. The laser radiation, absorbed by conduction electrons at the surface and transferred to the lattice by fast electron-phonon relaxation, is assumed to balance the inward heat flow. To find the resultant strain injected into the crystal, therefore, we first calculate the oscillatory part of the temperature distribution within the transducer by solving the heat diffusion equation with appropriate boundary conditions. The strain is subsequently derived from the acoustic wave equation with the oscillatory temperature distribution as source for thermoelastic expansion.

### A. Oscillatory temperature distribution

At the frequencies of interest, the length scale characteristic for diffusion of the oscillatory part of the heat, i.e., the thermal skin depth $\alpha^{-1}=(2\kappa/\omega)^{1/2}$, is very small ($\lesssim 0.2$ $\mu$m) in comparison with the diameter of the irradiated disk ($\approx 40$ $\mu$m). Here, $\kappa=K/C_V$ is the diffusivity, $K$ the thermal conductivity, and $C_V$ the specific heat of the transducer material. Unlike the inevitable steady-state heat, therefore, the problem of diffusion of the frequency-dependent heat may be treated as one-dimensional, so that the oscillatory part of the temperature, $\vartheta(z,t)$, satisfies the heat diffusion equation[1,14]

$$\frac{\partial^2 \vartheta(z,t)}{\partial z^2}-\frac{1}{\kappa}\frac{\partial \vartheta(z,t)}{\partial t}=0. \tag{1}$$

The oscillatory energy flux leaving the transducer is similarly governed by the, in comparison with the transducer, small heat conductivity of the crystal, which can be modeled by an effective heat conductivity $H$ across the interface. The boundary conditions at the free surface ($z=0$) and the transducer-crystal interface ($z=d$) thus read

$$K\partial \vartheta(z,t)/\partial z\big|_{z=0}=-\Phi_\omega \sin \omega t, \tag{2}$$

$$K\partial \vartheta(z,t)/\partial z\big|_{z=d}=-H\vartheta(d,t). \tag{3}$$

Equations (1)–(3) are amenable to rigorous analytic solution, but the result is quite complicated. In the relevant frequency range, however, $\alpha^{-1}$ does not exceed 200 nm, so that $h=H/K \ll \alpha$ (cf. the estimate of $h$ below.) In the limit of negligible thermal conductivity toward the crystal ($h=0$), the solution simplifies to

$$\vartheta_0(z)=\frac{\Phi_\omega}{\alpha K\sqrt{2}}\left(\frac{\cosh[2\alpha(d-z)]+\cos[2\alpha(d-z)]}{\cosh(2\alpha d)-\cos(2\alpha d)}\right)^{1/2}. \tag{4}$$

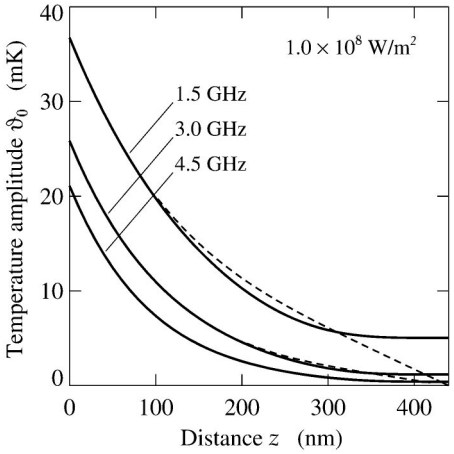


FIG. 2. The amplitude $\vartheta_0(z)$ of the oscillatory temperature inside the 440-nm-thick gold transducer, as calculated from Eq. (4) for various frequencies in the realistic limit of vanishing $h$. The dashed curves apply to infinite conductivity into the depth of the crystal ($h\to\infty$).

For an estimate of $\vartheta_0(z)$, we consider, as a case in point, an energy flux $\Phi_\omega=10^8$ W/m$^2$, such as provided by typically 100 mW of dye-laser power spread over a focus of about 20 $\mu$m radius. For gold at 300 K, $K=318$ W/m K and $C_V=2.5\times10^6$ J/m$^3$ K.[15] Figure 2 then shows the temperature distribution calculated from Eq. (4) at frequencies of 1.5, 3.0, and 4.5 GHz for vanishing conductivity toward the crystal ($h=0$). Near the surface of the transducer, the temperature modulation is found to be of order 30 mK, only weakly dependent on the thickness as long as $d>100$ nm. Also entered in Fig. 2, as the dashed curves, is the solution for $h\to\infty$, to show that differences in $h$ only show up at greater depths, where $\vartheta_0(z)$ has already diminished.

If the laser beams strike the transducer from the back side, i.e., at the interface with the crystal instead of at the free surface, Eq. (2) should be appropriately modified. The oscillatory temperature then reads as Eq. (4), except for the replacement of $d-z$ by $z$. From Eq. (4) and this result the temperature modulation is seen to be approximately inversely proportional to the square root of the modulation frequency.

Inevitably, the dye-laser illumination also causes steady-state heating. As thermal conduction is two orders of magnitude larger in gold than in the $PbMoO_4$ substrate [$K_{PbMoO_4}=1.5$ W/m K (Ref. 16)], the steady-state temperature is virtually uniform over the depth of the transducer. For an estimate, we therefore assume that the incident energy is supplied evenly over the focal area and carried away by diffusive heat transport outward into the nonilluminated parts of the Au film. From the appropriate Poisson equation,[17] the steady-state temperature then is found raised by $\Delta T=\Phi_0 w^2/8dK$ averaged over the heated disk, where $w$ is the focal radius and $d$ is the film thickness. For our case in point, i.e., $\Phi_0\approx10^8$ W/m$^2$, $w\approx20$ $\mu$m, and $d=440$ nm, we find $\Delta T\sim40$ K. The crystal, on the other hand, is not appreciably heated, as is borne out by the near absence of a rise in the thermal Brillouin signal. If the steady-state heat were to dif-

fuse exclusively into the semi-infinite substrate, a similar calculation would yield $\Delta T = 8\Phi_0 w/3\pi K_{PbMoO_4} \sim 1100$ K. The steady-state temperature rise so calculated is of course never reached because of the predominantly lateral flow, but may serve to quantify the thermal resistance across the interface. Balancing $\Phi_0$ to $H\Delta T$ gives $H \sim 10^5$ W/m$^2$K or $h \sim 6 \times 10^4$ m$^{-1}$.

### B. Acoustic wave

The temperature distribution $\vartheta(z,t)$ makes the transducer expand and contract along the $z$ direction, thereby producing a periodic thermal strain $\beta\vartheta(z,t)$, where $\beta$ is the linear thermal expansion coefficient. The stress thus amounts to $\sigma(z,t) = C[\varepsilon(z,t) - \beta\vartheta(z,t)]$,[6] in which $C$ is the relevant elastic constant, $\varepsilon(z,t) = \partial u(z,t)/\partial z$ is the elastic strain, $u(z,t)$ is the atomic displacement, and the indices distinguishing the components of $\sigma$, $C$, $\varepsilon$, and $u$ are omitted. Displacement and stress satisfy the equation of motion $\rho\,\partial^2 u(z,t)/\partial t^2 = \partial\sigma(z,t)/\partial z$ of an infinitesimal volume element with mass density $\rho$. Substitution of $\sigma$ and the relation $v = (C/\rho)^{1/2}$ for the sound velocity, then leads to the wave equation

$$\frac{\partial^2 u(z,t)}{\partial z^2} - \frac{1}{v^2}\frac{\partial^2 u(z,t)}{\partial t^2} = \beta\frac{\partial\vartheta(z,t)}{\partial z}. \tag{5}$$

In solving Eq. (5), we distinguish the transducer ($z<d$) and the crystal ($z>d$), the latter of which is assumed free of thermal strain. As is seen from Eq. (4), $\vartheta(z,t)$ is composed of contributions of the form $\Theta e^{-\gamma z} e^{i\omega t}$ and their complex conjugates, each of which adds two oppositely propagating traveling waves and an evanescent wave decaying with the depth to the solution of Eq. (5) within the transducer. Connected to these waves is a traveling wave propagating into the depth of crystal. The amplitudes of the three, longitudinally polarized, traveling waves are related to $\Theta$ by the boundary conditions, viz., the absence of stress at the free surface ($z=0$), and matching of displacements and stresses at the transducer-crystal interface ($z=d$). That is,

$$\partial u_1/\partial z|_{z=0} - \beta\Theta e^{i\omega t} = 0,$$

$$u_1|_{z=d} = u_2|_{z=d}, \tag{6}$$

$$C_1(\partial u_1/\partial z|_{z=d} - \beta\Theta e^{-\gamma d} e^{i\omega t}) = C_2\partial u_2/\partial z|_{z=d},$$

in which quantities pertaining to transducer and crystal are, when necessary, labeled with subscripts 1 and 2. By solving for the wave amplitudes and summing over $\Theta$, we find for the atomic displacement in the crystal

$$u_2(z,t) = \frac{\beta C_1 \Phi_\omega}{2\alpha K}\left(\frac{\mathcal{P}}{\mathcal{Q}}\right)^{1/2}\sin(\omega t - q_2 z + \varphi), \tag{7}$$

in which

$$\mathcal{P} = \cosh(2\alpha d) + \cos(2\alpha d) + 2\cos(q_1 d)[\cos(q_1 d) - 2\cosh(\alpha d)\cos(\alpha d)], \tag{8}$$

$$\mathcal{Q} = 2(1 + 4\alpha^4 q_1^{-4})[C_1^2 q_1^2 \sin^2(q_1 d) + C_2^2 q_2^2 \cos^2(q_1 d)] \times [\cosh(2\alpha d) - \cos(2\alpha d)], \tag{9}$$

with $q_1 = \omega/v_1$ and $q_2 = \omega/v_2$ representing the moduli of the wave vectors in the transducer and the substrate, and $\varphi$ denoting a phase angle. For the geometry with the laser beam incident at the back of the transducer, the solution is slightly more complex. It reads as Eq. (7) except that

$$\begin{aligned}\mathcal{P} = {} & 2 + \cos^2(q_1 d)[\cosh(2\alpha d) + \cos(2\alpha d)] \\ & - 4\cos(q_1 d)\cosh(\alpha d)\cos(\alpha d) + 4\alpha q_1^{-1}\sin(q_1 d) \\ & \times[\sinh(\alpha d)\cos(\alpha d) - \cosh(\alpha d)\sin(\alpha d)] \\ & - 2\alpha q_1^{-1}\cos(q_1 d)\sin(q_1 d)[\sinh(2\alpha d) - \sin(2\alpha d)] \\ & + 2\alpha^2 q_1^{-2}\sin^2(q_1 d)[\cosh(2\alpha d) - \cos(2\alpha d)].\end{aligned} \tag{10}$$

The amplitude of the elastic strain derived from Eq. (7) is $\varepsilon = q_2 u_{0,2}$, with $u_{0,2}$ the amplitude of $u_2(z,t)$. Given the strain, the acoustic power emitted per unit illuminated area of the transducer is finally derived from

$$P_{ac} = \tfrac{1}{2}\rho_2 v_2^3 \varepsilon^2, \tag{11}$$

in which the mass density $\rho_2$ and the longitudinal sound velocity $v_2$ pertain to the crystal. Note that the length scales contained in $P_{ac}$, viz., the acoustic wavelength $\lambda = 2\pi v/\omega$ and the thermal skin depth $\alpha^{-1} = (2K/\omega C_V)^{1/2}$, have different frequency dependences. Note furthermore that $P_{ac}$ is quadratic in $\Phi_\omega$. For $\Phi_\omega \sim 10^8$ W/m$^2$, $P_{ac}$ amounts to a few W/m$^2$, i.e., a conversion efficiency of order $10^{-8}$, in accordance with earlier estimates.[18]

### C. Experiments on thermomodulation

Experimental results of the Brillouin intensity versus the transducer thickness are, for a selection of phonon frequencies, shown in Fig. 3 for front-side and Fig. 4 for back-side laser-induced thermomodulation. The Brillouin detection was achieved at a distance close to the transducer ($\approx 0.1$ mm). In between data points, the joint dye-laser focus was moved from one transducer thickness step to the next by displacing the crystal transverse to the Brillouin-scattering plane. The signal intensities are normalized to the intensity of thermal Brillouin scattering, so that a comparison can be made from one thickness to the next. Also shown in Figs. 3 and 4, as the solid curves, are the theoretical results for $P_{ac}$ derived from Eqs. (7)–(11), where only vertical scaling has been applied. While each individual panel in Figs. 3 and 4 to some extent suffers from a scarcity of data points, an impressive agreement is found when combining the results for all frequencies and the two geometries.

According to Eqs. (7)–(11) the acoustic intensity depends on the thickness of the transducer. The intensity is in the first

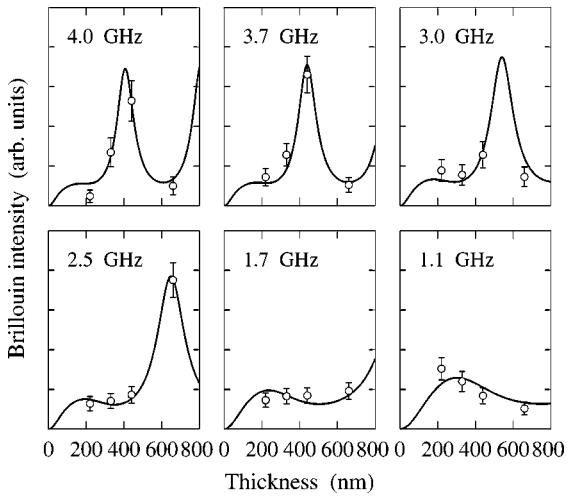


FIG. 3. The Brillouin intensity arising from longitudinal phonons generated by thermomodulation of the front surface of a gold transducer deposited on a (001) surface of a $PbMoO_4$ crystal. The six panels differ in phonon frequency. The solid lines represent the intensity calculated from Eqs. (7), (8), (9), and (11), with vertical scaling according to $1/\omega$. Experimental data for a particular frequency are adjusted vertically to fit the theory.

instance maximal for $d$ equal to a multiple of half the phonon wavelength $\lambda$. For longitudinal 2.5-GHz phonons in Au ($v=3.24$ km/s), we have $\lambda/2=650$ nm, close to the $d=660$ nm used in the experiments. Similarly, $\lambda/2=410$ nm at 4.0 GHz, comparable to $d=440$ nm. For front heating (Fig. 3), the strongest signals are indeed measured at these values. The transducer thus acts as a ''phonon interferometer'' with one totally and one partly reflecting mirror. In the time domain, a related experiment has been performed by Thomsen *et al.*,[6] who used a picosecond laser to generate a pulsed strain. A series of equally spaced pulses was observed, corresponding to successive round trips of the acoustic pulse in the film. If the transducer is illuminated at the

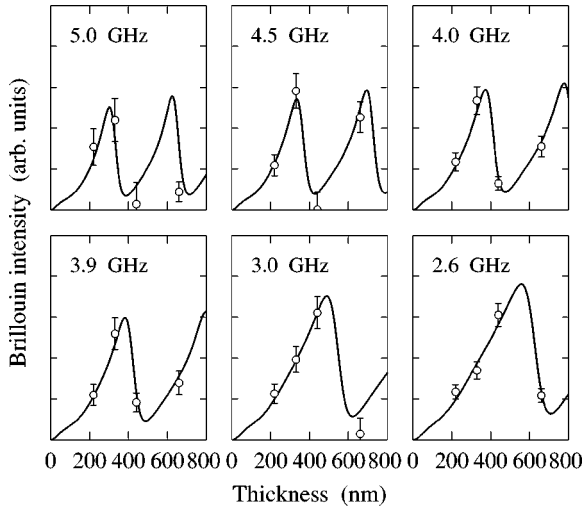


FIG. 4. Same as Fig. 3, but excitation at the back side of the transducer. In calculating the solid lines Eq. (10) is used in lieu of Eq. (8).

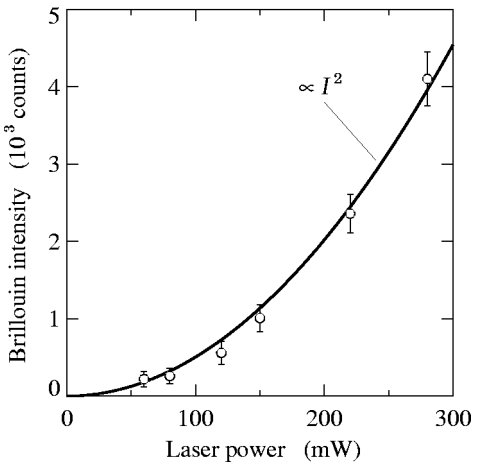


FIG. 5. The Brillouin intensity at $\omega/2\pi=2.5$ GHz vs the incident laser power. The solid line represents the quadratic dependence of the acoustic power on the incident laser power [cf. Eqs. (7) and (11)].

crystal side (Fig. 4), on the other hand, the acoustic intensity peaks at a significantly lower thickness, while at the same time the form of the resonance has become asymmetric.

Equations (7)–(11) furthermore predict that the acoustic power is proportional to the square of the incident laser power. This is confirmed by a separate experiment in which the Brillouin intensity is measured versus the incident laser power. The results are displayed in Fig. 5. In summary, the results in Figs. 3 and 4 for the thickness dependence combined with those in Fig. 5 for the laser-power dependence confirm the adequacy of the above theoretical description for phonon generation by thermomodulation of a thin metallic transducer.

For an assessment, in retrospect, of which material to choose as transducer, it is helpful to calculate $P_{ac}$ in the limit $\alpha d \gg 1$ and to rewrite the result in terms of the material properties[15] and the frequency by the substitutions $\alpha=(\omega C_V/2K)^{1/2}$, $q_1=\omega/v_1$, and $q_2=\omega/v_2$. Here, we have to distinguish between, on the one hand, the case $\rho_2 v_2<\rho_1 v_1$ or $C_2 q_2<C_1 q_1$ and the case $\rho_2 v_2>\rho_1 v_1$ on the other. In the former case, applicable to this paper, the condition of a node at the interface, $q_1 d=n\pi$, gives the best signal, whereas in the latter case an antinode, $q_1 d=(n+\frac{1}{2})\pi$, is to be favored [cf. Eq. (9)]. For $q_1 d=n\pi$ we find that $P_{ac}=\eta\Phi_\omega^2/8\rho_2 v_2$, where $\omega$ and the material constants of the transducer are collected into

$$\eta=\frac{\rho_1^2\beta^2 K\omega}{C_V^3(1+K^2\omega^2/C_V^2 v_1^4)}, \tag{12}$$

so that $\eta$ is a measure of the generation efficiency. Equation (12) holds for both front- and back-side excitation. The maximum $\eta=\rho_1^2\beta^2 v_1^2/2C_V^2$ is reached for $\omega_{max}=C_V v_1^2/K$ or $q_1=\alpha\sqrt{2}$. Gold, for which $\omega_{max}/2\pi=13$ GHz, turns out to be an excellent choice for the frequencies accessible by Brillouin detection. For $q_1 d=(n+\frac{1}{2})\pi$ and front-side excitation, $\eta$ is modified from Eq. (12) by a factor $(\rho_2 v_2/\rho_1 v_1)^2$. For $q_1 d=(n+\frac{1}{2})\pi$ and back-side excitation, $\eta$ should be multi-

plied by $(\omega_{\max}/\omega)(\rho_2 v_2/\rho_1 v_1)^2$ [cf. Eq. (10)], which makes back-side excitation preferable below $\omega_{\max}$ in case $\rho_2 v_2 > \rho_2 v_1$.

As to the temperature dependence of the generation efficiency, $\eta$ changes only moderately when the sample is cooled despite the decline of $\beta$ and $C_V$ toward cryogenic temperatures. The effects of cooling are apparently mitigated by the fact that thermal expansion scales with the lattice energy,[19] whence $\beta$ follows the temperature dependence of $C_V$. A further circumstance reducing the temperature dependence is that the steady-state temperature prevailing below the illuminated spot remains at some 40 K (cf. Sec. III A), so that $\beta$, $C_V$, and $K$ do not attain their low-temperature limits. Furthermore, $K$ is likely to be governed by impurity and boundary scattering,[20] differently from pure bulk metals, where dwindling anharmonic phonon processes first cause $K$ to increase according to $T^{-2}$ before impurity scattering takes over.[19] The weak sensitivity of $\eta$ on the sample temperature all the way down to the cryogenic regime considerably simplifies matters when applying the present technique to the measurement of phonon decay versus the temperature.[21]

## IV. PROPAGATION

### A. Fresnel diffraction

For a quantitative description of the divergence of the acoustic beam by diffraction, we consider a coherent wave emitted by the thermomodulated spot on the transducer and, by analogy, resort to the physical optics of light passing through a circular aperture. Wishing to calculate the diffracted strain in the Fresnel as well as the Fraunhofer regimes,[22] we choose as starting point the generalized Kirchhoff integral for Dirichlet boundary conditions

$$\varepsilon(x,y,z)=\frac{1}{2\pi i}\int\int_{\mathcal{O}}\varepsilon(x',y',0)\frac{e^{-iqR}}{R}q\left(1+\frac{i}{qR}\right)\times\frac{\mathbf{n}\cdot\mathbf{R}}{R}dx'dy', \tag{13}$$

where, in the present context, $\varepsilon(x,y,z)$ is to be identified with the strain in lieu of the optical electric field, $q$ is the modulus of the acoustic wave vector, $\mathbf{n}$ is the normal unit vector, and the vector $\mathbf{R}$ connects the surface element $dx'dy'$ at position $(x',y',0)$ on the transducer with the point of observation $(x,y,z)$ in the crystal. Note that $q$ is connected to the acoustic angular frequency $\omega$ through the anisotropic dispersion relation $\omega(\mathbf{q})$. The Kirchhoff integral, Eq. (13), indeed enables us to evaluate the strain at any position $(x,y,z)$ in the crystal from a given distribution $\varepsilon(x',y',0)$ in the plane $\mathcal{O}$ of the transducer $(z=0)$. As no sources are present inside the crystal, it is considered justified to apply Eq. (13) to the individual components of a tensor such as the strain, although Eq. (13) has strictly speaking been derived for a scalar field. Also, Dirichlet boundary conditions are more convenient than the more common Kirchhoff boundary conditions or, for that matter, Neumann boundary conditions, because no knowledge of $\nabla\varepsilon(x',y',0)$ is required in addition to $\varepsilon(x',y',0)$.

In comparison with a uniformly illuminated circular aperture in optics, however, the present situation is more complex. First, the acoustic intensity profile leaving the transducer, which is proportional to the Gaussian-shaped optical intensity distribution squared (cf. Fig. 5), likewise is Gaussian, yet with a $\sqrt{2}$ times smaller width. Second, the phase of the acoustic wave leaving the transducer is not necessarily uniform over the illuminated area. It depends on the local phase of the optical modulation, which in turn depends on the phase profiles of the dye-laser wave fronts. Third, the group velocity generally deviates in direction from the wave vector as a result of elastic crystalline anisotropy. This effect is commonly known as phonon focusing. Prior to working out Eq. (13), we need to consider these complications in some detail.

The optical electric field in the focal waist of a laser beam has been treated in terms of standard diffraction theory.[23,24] If $k$ is the wave vector of the laser light, propagating in the positive $z$ direction, and if $\omega_l$ is its angular frequency, then the amplitude of the optical electric field near the waist is given by

$$E(x,y,z)\propto\frac{W_0}{W}e^{-r^2/W^2}e^{i(\omega_l t-kz-kr^2/2L-\psi)}, \tag{14}$$

which depends on $x$ and $y$ only through the distance $r=(x^2+y^2)^{1/2}$ from the optical axis; $z$ is the distance along this axis from the focal center. We further have

$$W(z,\mathcal{R}_{\rm opt})=W_0[1+(z/\mathcal{R}_{\rm opt})^2]^{1/2}, \tag{15}$$

$$L(z,\mathcal{R}_{\rm opt})=z[1+(\mathcal{R}_{\rm opt}/z)^2], \tag{16}$$

and $\psi=\arctan(z/\mathcal{R}_{\rm opt})$, with $\mathcal{R}_{\rm opt}=\frac{1}{2}kW_0^2$ the Rayleigh range. The quantity $W$ represents half the $1/e$ waist diameter, with $W_0$ half the $1/e$ diameter at the narrowest point. The radius of curvature $L$ of the wave front intersecting the optical axis at $z$ attains its minimum value $2\mathcal{R}_{\rm opt}$ for $z=\mathcal{R}_{\rm opt}$. In Eq. (14), it is assumed that $W\ll\mathcal{R}_{\rm opt}$, whence $E(x,y,z)$ varies only slowly with $z$.

Starting from Eq. (14) for a single laser beam, we make up the intensity distribution $I(x',y',0)$ at the transducer as a result of the two interfering Gaussian beams. Positioning the transducer at $z=0$, we allow shifts of the two waists along the optical axis to distances $d_1$ and $d_2$ from the transducer. We thus have $I_{\rm opt}(x',y',0)=|E_1(x',y',d_1)+E_2(x',y',d_2)|^2$. Upon omitting terms leading to steady-state heating or a uniform phase shift, the optical intensity at the transducer amounts to

$$I_{\rm opt}(x',y',0)\propto\frac{W_{0,1}W_{0,2}}{W_1W_2}e^{-(W_1^{-2}+W_2^{-2})r'^2}e^{i[\omega t-(k_1/2L_1-k_2/2L_2)r'^2]}, \tag{17}$$

where $k_1$, $W_{0,1}$, $W_1=W(d_1,\mathcal{R}_{\rm opt,1})$, $L_1=L(d_1,\mathcal{R}_{\rm opt,1})$, and their counterparts indexed by 2 refer to the two laser beams, $r'=(x'^2+y'^2)^{1/2}$, and adding the complex conjugate is implied. We henceforth drop the index to $k$, noting that $k_1$

$=k_2$ for all practical purposes. Also note that the optical angular difference frequency $\omega=\omega_1-\omega_2$ may be of either sign, but for convenience we adopt $\omega_1>\omega_2$.

The phase factor occurring in Eq. (17) has a circularly symmetric radial dependence identical to the transmission function $e^{iqr'^2/2f}$ of a lens of focal length $f$, where in the present context $q$ is to be identified with the acoustic wave vector.[25] Accordingly, we may rewrite Eq. (17) as

$$\varepsilon(x',y',0)=\varepsilon_0 e^{-r'^2/w_0^2} e^{i(\omega t+qr'^2/2f)}, \tag{18}$$

placing an acoustic lens of focal length

$$f=\frac{qL_1L_2}{k(L_1-L_2)} \tag{19}$$

at $z=0$ and collecting into the constant $\varepsilon_0$ all prefactors occurring in Eq. (17) as well as the proportionality constant connecting $\varepsilon(x',y',0)$ to $I_{\rm opt}(x',y',0)$ [cf. Eq. (7)]. The quantity $w_0$, defined by $w_0^{-2}=W_1^{-2}+W_2^{-2}$, represents the initial $1/e$ radius of the acoustic beam. Note that $f$ depends linearly on $\omega$ through $q$. Only in case $L_1=L_2$ do we have $f\to\infty$ and are the laser wave fronts of equal phase over the entire irradiated spot. In case the optical waists are equally narrow, $f$ reaches its smallest value $q\mathcal{R}_{\rm opt}/k$ for $d_1=-d_2=\mathcal{R}_{\rm opt}$ [cf. Eq. (16)].

We next turn to the effects of phonon focusing on Fresnel diffraction. Phonon focusing, or in the present case defocusing, is caused by the elastic anisotropy. Extensive experiments have been carried out, all confirming theory,[8–10] in particular with phonon imaging,[26] using bolometers,[27] tunnel junctions,[28] and scanning electron microscopy[29] as phonon detectors. Phonon focusing is best visualized in terms of the slowness surface, i.e., the locus in $\mathbf{q}$ space of the slowness vector $\mathbf{S}(\mathbf{q})=\mathbf{q}/\omega(\mathbf{q})$. Anisotropy makes the group velocity $\mathbf{v}_g(\mathbf{q})=\nabla_{\mathbf{q}}\omega(\mathbf{q})$, which points along the surface normal, differ in direction from the phase velocity $\mathbf{v}_{\mathbf{q}}=[\omega(\mathbf{q})/q]\mathbf{e}_{\mathbf{q}}$.

For small angles from a principal direction, the slowness surface may be approximated by a paraboloid of revolution and the focusing effect accommodated into a single material parameter changing the modulus of $\mathbf{q}$ with the angle. That is,

$$q=q_c(1-p\theta_{\mathbf{q}}^2), \tag{20}$$

in which $\theta_{\mathbf{q}}$ is the angle of $\mathbf{q}$ from the $c$ axis and $q_c=\omega/v_c$ is the modulus of $\mathbf{q}$ along this axis. The focusing parameter $p$ may be expressed in the elastic constants by comparing Eq. (20) with the relevant algebraic solution of the Christoffel equation.[10,30] For longitudinal acoustic phonons propagating in directions near a fourfold $c$ axis, this yields[31]

$$p=\frac{C_{13}^2+2C_{13}C_{44}+2C_{33}C_{44}-C_{33}^2}{2C_{33}(C_{33}-C_{44})}. \tag{21}$$

The elastic constants of $PbMoO_4$ are, in units $10^{11}$ N/m$^2$ and in the customary two-index notation,[30] $C_{11}=1.092$, $C_{33}=0.917$, $C_{44}=0.267$, $C_{66}=0.337$, $C_{12}=0.683$, $C_{13}=0.528$, and $C_{16}=-0.136$.[16,32] The constant $C_{33}$ is related to the velocity $v_c$ of longitudinal sound along the $c$ axis through $v_c=(C_{33}/\rho)^{1/2}=3.63$ km/s.[16] These numbers yield $p=+0.176$, i.e., defocusing. Equation (20) is adequate up to several tens of degrees from the $c$ axis. At $\theta_{\mathbf{q}}=20°$, for example, the true decrease of $q$ from $q_c$ is 1.9%, compared to 2.1% according to Eq. (20).

At this stage, we combine diffraction with phonon focusing and the acoustic lens representing the laser irradiance profile by inserting Eqs. (18) and (20) into Eq. (13), using the identity $\theta_{\mathbf{q}}=\arctan\{[(x-x')^2+(y-y')^2]^{1/2}/z\}$ to express $\theta_{\mathbf{q}}$ in the planar coordinates $\mathbf{r}=(x,y)$ within the "screen" of observation and $\mathbf{r}'=(x',y')$ within the transducer. We subsequently expand all phase angles up to second order in $x$, $y$, $x'$, and $y'$, but retain the remainder of the integrand in Eq. (13) to lowest order only. Introducing the abbreviation $Q=q_c(1-2p)/2z$, we then find for the diffracted strain in the Fresnel approximation

$$\varepsilon(x,y,z)=\frac{q_c\varepsilon_0}{2\pi iz}e^{i(\omega t-q_cz-Qr^2)}\int\!\!\int_{\mathcal{O}} e^{-r'^2/w_0^2} \times e^{i[q_cr'^2/2f-Q(r'^2-2xx'-2yy')]}dx'dy'. \tag{22}$$

The experiments below only sense the modulus of the strain, for which integration of Eq. (22) yields the simple expression

$$|\varepsilon(x,y,z)|=\varepsilon_0\frac{w_0}{w}e^{-r^2/w^2}. \tag{23}$$

Here, the quantities

$$w(z)=w_0\left[\left(1-\frac{z}{f'}\right)^2+\left(\frac{z}{\mathcal{R}'}\right)^2\right]^{1/2}, \tag{24}$$

$$\mathcal{R}'=\tfrac{1}{2}q_cw_0^2(1-2p), \tag{25}$$

$$f'=f(1-2p) \tag{26}$$

represent the $1/e$ radius of the acoustic beam at distance $z$, the elasticity-modified acoustic Rayleigh range, and the elasticity-modified focal length, respectively. Phonon focusing ($p<0$) or defocusing ($p>0$) thus turns out to stretch or shrink all length scales by a factor of $1-2p$. It is a simple task to derive the equivalents of Eqs. (24)–(26) for phonon focusing along other directions.

### B. Experiments on the divergence

The divergence was measured at frequencies ranging from 1.2 to 4.0 GHz or acoustic wavelengths ranging from 3.0 to 0.9 $\mu$m. These wavelengths are sufficiently large in relation to the generating spot to achieve diffraction angles of order 1°–4° to either side. No precaution was taken to equalize the phase distributions of the dye-laser beams, so that a finite $f$ is anticipated. Experiments in which, with the help of additional optics, the phase difference is made uniform or maximal acoustic focusing is achieved are deferred to Sec. IV C.

The experiments entail measuring the lateral profile of the phonon beam at various distances $z$ from the generating spot.

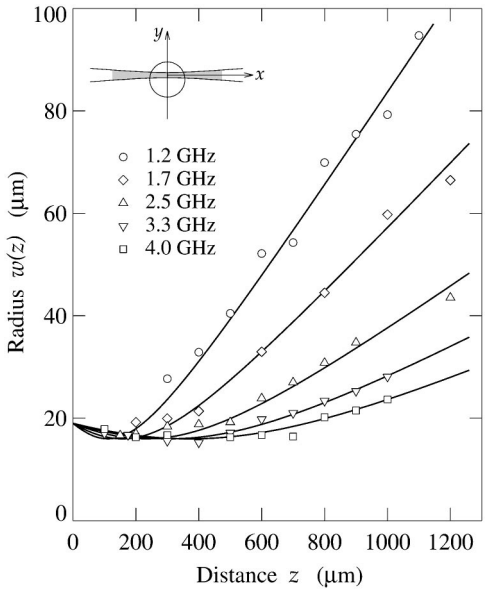


FIG. 6. The $1/e$ intensity radius $w(z)$ of the acoustic beam, corrected for the finite detection volume with the help of Eq. (27), as a function of the distance from the transducer for various phonon frequencies. The curves are fits of $w(z)$ according to Fresnel diffraction. The inset depicts the Brillouin-scattering geometry. The acoustic beam is viewed head-on, while the primary Brillouin beam enters from the side. The detection volume is pencil shaped along the $x$ direction and scanned in the $y$ direction to measure the acoustic profile.

To derive $w(z)$ from the measured Brillouin profiles, however, corrections must be made for the finite detection volume, an elongate pencil completely traversing the acoustic beam (inset to Fig. 6) and possessing a Gaussian cross section defined by the focused primary Brillouin laser light. Brillouin scattering scales with $|\varepsilon(x,y,z)|^2$, which in the present geometry drops as $\exp[-2(x^2+y^2)/w^2]$ with increasing distance from the acoustic axis ($z$ axis), while varying only slowly along the acoustic beam [cf. Eq. (23)]. Integrated over the detection volume, the measured Brillouin profile thus is proportional to $2ww_Bw_me^{-(y/w_m)^2}$, in which $w_B$ is the $1/e$ intensity radius of the Brillouin laser beam and $w_m$ is given by

$$w_m=(\tfrac{1}{2}w^2+w_B^2)^{1/2}. \tag{27}$$

Sets of lateral Brillouin profiles at various distances $z$ were measured for 1.2, 1.7, 2.5, 3.3, and 4.0 GHz. To leave the Brillouin spectrometer undisturbed once tuned to a certain frequency, scanning along the $y$ axis was realized by raising or lowering the dye-laser focus above or below the Brillouin-scattering plane via sideways shifts of the focusing lens. In analyzing these data, first each profile is characterized by its measured width $w_m$ through fits of a Gaussian augmented with a small background. These backgrounds turn out to compare with the Brillouin signal in the absence of thermomodulation and, accordingly, are due to thermal phonons only. Next, Eq. (27) with Eqs. (24)–(26) substituted is fitted to all $w_m$ so obtained, to find $w_0$, $f$, and $w_B$. Note that $p$ and $q_c=\omega/v_c$ are known. In the fits, $f$ was taken to scale with $\omega$ [cf. Eq. (19)], whereas a universal $w_0$ was adopted. Because the Brillouin spectrometer requires realignment from one $\omega$ to the next, an independent $w_B$ was chosen for each set of $w_m$ versus $z$.

The results for $w$ as a function of $z$, i.e., the divergence of the acoustic power corrected for the finite Brillouin detection volume, are shown in Fig. 6. The fitted parameters are $w_0=19\pm1$ μm and $f=1.94\pm0.20$ mm at 4.0 GHz, while $w_B$ is in the range 2–7 μm. According to Eq. (19) the minimum $f$ amounts to 0.7 mm at 4.0 GHz, so that the acoustic lens is relatively weak. The lower limit of $w_B$ matches the diffraction-limited 2-μm radius of the Gaussian-shaped Brillouin laser beam in the detection volume.[23,24] The curves in Fig. 6 represent Eqs. (24)–(26) with the fitted parameters inserted. They faithfully track the data over a substantial range of distances and frequencies for a unique $w_0$, thereby showing how well the divergence of the acoustic beam with due account of phonon focusing conforms to Fresnel diffraction from a circular spot.

### C. Experiments on the acoustic lens

We next vary the radial phase distribution of the thermomodulation. In Sec. IV A we have shaped this distribution into the form of an acoustic lens positioned just below the transducer. We first consider the case of a flat phase profile, achieved by making the waists of the dye-laser beams coincident with the transducer ($d_1=d_2=0$). As these waists are images of the intrinsic beam waists of the dye lasers,[33] their shifts can be effected by suitable modification of the optical path lengths. Representative data taken under these conditions at $\omega/2\pi=5.6$ GHz are presented in Fig. 7(a). Indeed, no acoustic lens is found. The solid curve in Fig. 7(a) represents a successful fit of Eq. (24) with $f$ set to infinity. Fitting further yielded $w_0=17\pm1$ μm, $w_B\lesssim5$ μm, and a lower bound of 8 mm for $f$.

In further experiments, one optical path was lengthened and the other one shortened, so that the imaged waists are shifted to either side of the transducer surface by about 1 mm. The acoustic beam now narrows at first, only to diverge at larger distances. A representative example, in which the initial narrowing is about the strongest, is presented in Fig. 7(b). As in the lens-free case, Fig. 7(a), the solid curve represents a fit of Eq. (24), now yielding $f=1.0\pm0.2$ mm and $w_0=19\pm1$ μm. Note that $w_0$ is somewhat larger than in Fig. 7(a) because the waists have shifted. From Eq. (24) the initial dependence of $w(z)$ on $z$ reads

$$w(z)=w_0(1-z/f'), \tag{28}$$

which in Figs. 7(a) and 7(b) is indicated with thin straight lines. Indeed, the short focal length $f$ found in Fig. 7(b) corresponds, within the uncertainties, to the minimum $f=q\mathcal{R}_{\rm opt}/k$ achievable according to Eq. (19) for $d_1=-d_2=\mathcal{R}_{\rm opt}$. In an independent experiment, the $1/e$ radii of the imaged dye-laser waists were determined by measuring the light intensity transmitted through pinholes. The results are $W_{0,1}=15\pm2$ μm and $W_{0,2}=18\pm2$ μm. Adopting the aver-

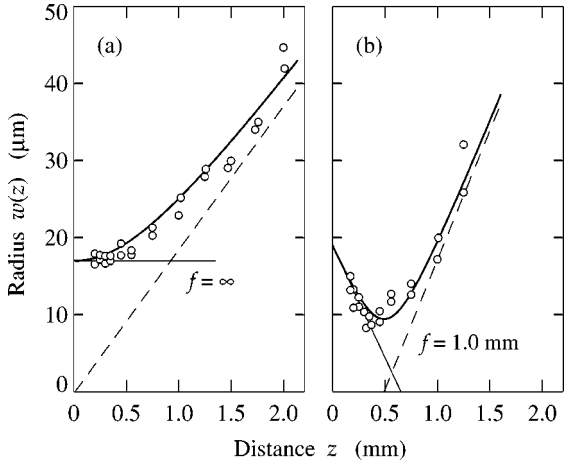


FIG. 7. The $1/e$ intensity radius $w(z)$ of the acoustic beam, corrected for the finite detection volume, as a function of the distance from the transducer at a phonon frequency $\omega/2\pi = 5.6$ GHz. For data set (a), showing absence of focusing, the waists of the laser beams coincide with the transducer surface. For data set (b), the waists are positioned such that maximum focusing of the acoustic beam is achieved [cf. Eq. (19)]. The solid lines represent Eqs. (24)–(26) with $f$ as indicated, the thin straight lines the corresponding initial dependence according to Eq. (28), and the dashed lines the asymptotic dependence according to Eq. (29). The sample temperature is 2.1 K.

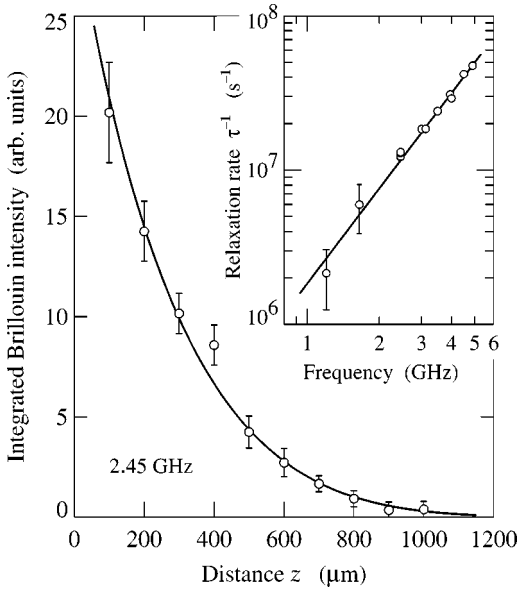


FIG. 8. The Brillouin intensity integrated over the cross section of the acoustic beam in $PbMoO_4$ at room temperature vs the distance $z$. The main plot gives, as representative example, the results for 2.45-GHz phonons. The solid curve is a single-exponential decay [cf. Eq. (30)], corrected for incomplete integration over $x$ at higher $z$. The inset shows the relaxation rate $\tau^{-1}$ vs the frequency $\omega/2\pi$, the straight line representing Eq. (31).

age for $W_0$, we find $\mathcal{R}_{\rm opt} = 1.4 \pm 0.3$ mm, and $f = 1.2 \pm 0.3$ mm for the strongest possible acoustic lens at 5.6 GHz.

In comparing Fig. 7(a) to Fig. 7(b), it is of interest to note that the phase differences over the illuminated spot are quite limited. At a distance $w_0$ from the center, for example, the phase is only $q_c w_0^2/2f \approx 100°$ ahead, i.e., by less than half a period. Second, the condition of uniform phase as in Fig. 7(a) not only results in the smallest $w_0$, but also in minimum divergence of the acoustic beam at larger distances. From Eq. (24) it is readily seen that the asymptotic $1/e$ acoustic radius reads

$$w(z) = w_0 \frac{(f'^2 + \mathcal{R}'^2)^{1/2}}{\mathcal{R}'} \left( \frac{z}{f'} - \frac{\mathcal{R}'^2}{f'^2 + \mathcal{R}'^2} \right), \qquad (29)$$

whose slope is indeed minimum for $f' \to \infty$. For a comparison, Eq. (29) has been entered as the dashed lines in Fig. 7.

### D. Phonon decay

The decay of the Brillouin intensity with distance contains information on the damping of the acoustic wave or, in the terminology preferred in this context, the relaxation of the phonons with time. The Brillouin intensity scales with the local density of phonons sharing the detection volume, so we have to integrate the Brillouin intensity over the cross section of the acoustic beam to find the total number of phonons left at distance $z$. Note that phonons escape Brillouin detection once they have engaged in scattering. The detection volume being pencil shaped, integration is implied in the horizontal direction. To compare the total number of phonons in the acoustic beam from one position to the next, therefore, we integrate over vertical Brillouin intensity profiles such as the ones measured in connection with Figs. 6 and 7. To eliminate drift in the detection sensitivity, the intensities were calibrated with reference to the thermal background.

Brillouin intensity profiles of the acoustic beam have been measured versus the distance $z$ for a set of frequencies in the range $\omega/2\pi = 1.2$–$4.9$ GHz. For the representative example of 2.45-GHz phonons, their integrated intensities are displayed in Fig. 8. As anticipated, the Brillouin intensity drops exponentially with $z$. In the detailed data analysis, the Brillouin intensity is taken to depend on the time $z/v$ elapsed since the phonons left the transducer according to the single-exponential decay

$$I = I_0 e^{-z/v\tau}, \qquad (30)$$

in which $\tau$ is the relaxation time. With inclusion of a correction accounting for incomplete integration over the widened acoustic beam at large $z$, Eq. (30) is indeed found to faithfully track the data points (solid curve in Fig. 8). In the inset to Fig. 8, the fitted results for the relaxation rate $\tau^{-1}$ are displayed double logarithmically as a function of the phonon frequency and seen to follow a power law.

As to the question of what frequency dependence to expect, Herring[34] has argued that in real crystals, which are elastically anisotropic, the relaxation is quite different from isotropic approximations. Applying topological and group-theoretical considerations to the slowness surfaces, he in particular showed that the relaxation of longitudinal acoustic phonons is dominated by wave-vector and energy-conserving processes in which the relaxing longitudinal phonon com-

bines with a thermal slow transverse phonon to form a fast transverse phonon. In the limit of small wave vectors, the associated relaxation rate should depend on the angular frequency $\omega$ and the temperature $T$ according to

$$\tau^{-1} = B\omega^a T, \tag{31}$$

provided the majority of the phonon modes have become thermally excited, i.e., at a sizable fraction of the Debye temperature. For crystals having $C_{4h}$ symmetry, such as $PbMoO_4$, Herring finds the asymptotic value $a=2$ for longitudinal phonons traveling along the tetragonal axis ($c$ axis). Returning to the results for $\tau^{-1}$ at $T=295$ K presented in the inset to Fig. 8, we find Eq. (31) to conform with experiment for $a=2.05\pm0.10$ and $B=(5.1\pm0.5)\times10^{-17}$ $s^{a-1}K^{-1}$, the latter value exclusive of the error propagated from $a$. The present experimental results therefore confirm Herrings's theory for phonon relaxation in anisotropic media.

### E. Measurement of phonon focusing

Another experiment demonstrating that the optical phase pattern is transferred to the phonon beam is to illuminate the transducer by a sideward moving grating, such as achieved when the interfering dye-laser beams are incident at a mutual angle. The moving optical grating induces a moving temperature grating in the focal area. The associated transverse wave vector translates into a lateral component of the strain wave injected into the crystal, so that the acoustic beam is deflected away from the $c$ axis. Note that the grating, owing to its sinusoidal intensity distribution, fails to emit side maxima, as distinct from the grating formed by a transducer made up of uniform stripes.[35] A complication over standard optics is that phonon focusing makes the group velocity differ in direction from the phase velocity when the phonon beam deviates from the $c$ axis. Brillouin scattering allows independent measurement of these velocities, the phase velocity by tilting the crystal until $\mathbf{q}$ lies in the Brillouin scattering plane, and the group velocity by measuring the angle for which maximum intensity is observed.

If the optical wave vectors of the incident dye-laser beams, $\mathbf{k}_1$ and $\mathbf{k}_2$, are at angles $\alpha_1$ and $\alpha_2$ from the surface normal, the strain at the transducer $\varepsilon(x',y',0)$ is specified by Eq. (18), yet multiplied by an additional phase factor $e^{ik_y y'}$. Ignoring the minute difference between the moduli $k_1$ and $k_2$, we have

$$k_y = k(\sin\alpha_1 - \sin\alpha_2). \tag{32}$$

Coincident beams thus produce no grating whatever their angle of incidence and, therefore, no sideward propagation of the acoustic beam. Already for $|\alpha_1-\alpha_2|\sim1°$, however, the grating period $2\pi/k_y$ is smaller than the $1/e$ diameter of the focus ($\approx40$ $\mu$m).

The experimental geometry is adapted to the experiment by tilting the crystal away from the Brillouin-scattering plane and running the dye-laser beams in parallel at some distance prior to focusing to a joint focus on the transducer (inset to Fig. 9). One dye-laser beam propagates along the optical axis

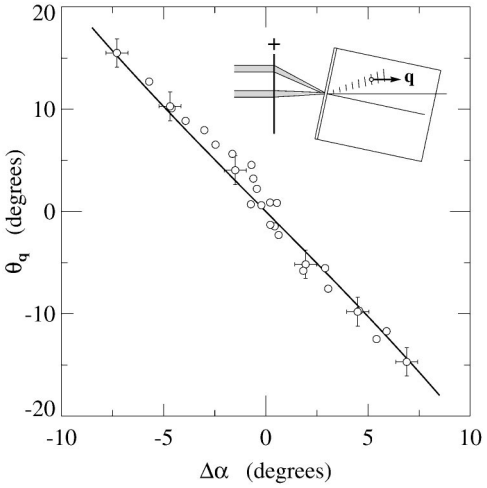


FIG. 9. The angle $\theta_{\mathbf{q}}$ of the phase velocity as a function of the angle $\Delta\alpha$ between the dye-laser beams at $\omega/2\pi=3.1\pm0.1$ GHz. The curve represents Eq. (33) without adjustable parameters. The inset shows the geometry, with $\mathbf{q}$ lying in the Brillouin-scattering plane.

of the focusing lens (focal length $F=80$ mm), and its angle of incidence $\alpha_1$ therefore equals the angle over which the crystal is tilted. The other beam is incident at an angle $\Delta\alpha=\alpha_1-\alpha_2$ from the former, where $\Delta\alpha$ derives from the distance $D$ between the laser beams through $\Delta\alpha=\arctan(D/F)$, apart from corrections up to 5% for longitudinal spherical aberration. Further, to allow for divergence of the group and phase velocities, the joint dye-laser focus is shifted by a distance $y$ out of the Brillouin-scattering plane until the acoustic beam passes through the detection volume. In the experiments, $\alpha_1$ and $y$ are repeatedly optimized to obtain maximum Brillouin signal for a given $\Delta\alpha$. The optimum $\alpha_1$ is to be identified with the angle $\theta_{\mathbf{q}}$ of the acoustic phase velocity. Results for $\theta_{\mathbf{q}}$ as a function of $\Delta\alpha$, the primary variable of the experiment, are presented in Fig. 9 for $\omega/2\pi=3.1\pm0.1$ GHz.

To express $\theta_{\mathbf{q}}$ in $\Delta\alpha$, we equate the wave vector of the moving grating to the component of the acoustic wave vector parallel to the transducer, i.e., $k_y=q\sin\theta_{\mathbf{q}}$. This condition results in an implicit equation for $\theta_{\mathbf{q}}$ when substituted in Eq. (32) along with $q$ according phonon focusing [Eq. (20)] and the optimized angles $\alpha_1=\theta_{\mathbf{q}}$ and $\alpha_2=\theta_{\mathbf{q}}+\Delta\alpha$. Treating the leading term rigorously and expanding the remainder in $\Delta\alpha$, we arrive at

$$\theta_{\mathbf{q}} = -A[1+\tfrac{1}{2}(1+2p)A^2]. \tag{33}$$

$$A = \arctan\left(\frac{(kv_c/\omega)\sin\Delta\alpha}{1-2(kv_c/\omega)\sin^2\tfrac{1}{2}\Delta\alpha}\right). \tag{34}$$

Restricting Eq. (33) to the dominant linear term gives the more transparent expression $\theta_{\mathbf{q}}=-(kv_c/\omega)\Delta\alpha$. Equation (33) is more detailed in that it includes corrections for the geometry and phonon focusing upon rotating $\mathbf{q}$ away from the $c$ axis. Returning to the experimental results for $\theta_{\mathbf{q}}$, we insert Eq. (33) into Fig. 9. The comparison turns out to be of

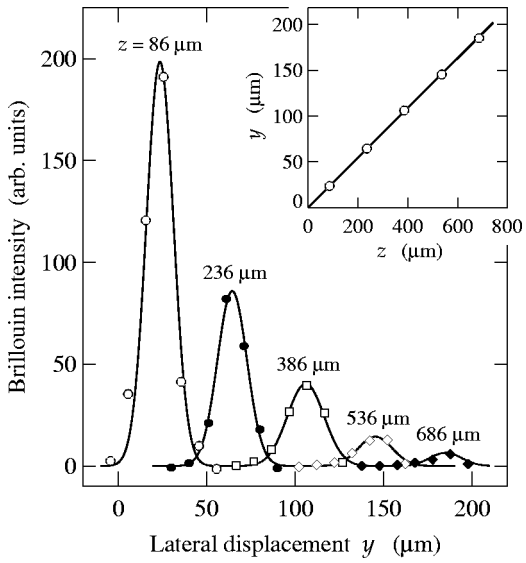


FIG. 10. Lateral intensity profiles of the acoustic beam for various distances $z$ below the transducer and a fixed $\Delta\alpha=-5.7°\pm0.5°$. The phonon frequency is $3.1\pm0.1$ GHz. Thermal background has been subtracted. The lateral displacement $y$ is measured with reference to the illuminated spot. The solid lines are least-squares-fitted Gaussians. The position of maximum intensity shifts faster with increasing $z$ than predicted by the phase velocity, indicating phonon defocusing. The inset shows $y$ vs $z$, yielding $\theta_g=15.7°\pm0.4°$ for the group velocity.

good quality despite the fact that all parameter values are known from other sources: $\omega/2\pi=3.1$ GHz, $k=2\pi/\lambda$, with $\lambda=580.0\pm0.1$ nm the optical wavelength, and $v_c=3.63$ km/s.

To arrive at an experimental value of $\theta_g$, lateral Brillouin intensity profiles have been collected at a series of distances from the transducer. The results are displayed in Fig. 10 for $\omega/2\pi=3.1\pm0.1$ GHz, $\Delta\alpha=-5.7°\pm0.5°$, and an optimized $\alpha_1=\theta_{\mathbf{q}}=11.5°$. The maxima of these profiles trace the course the acoustic energy travels into the crystal, and indeed the lateral displacement grows linearly with the distance (cf. inset to Fig. 10). We thus find $\theta_g=15.7°\pm0.4°$, inclusive of the corrections noted in connection with Eq. (33). The experimental result is to be compared with the angle $\theta_g$ of the normal to the slowness surface at a given $\theta_{\mathbf{q}}$ [cf. Eq. (20)]. We find

$$\theta_g=\theta_{\mathbf{q}}+\arctan\left(\frac{2p\,\theta_{\mathbf{q}}}{1-p\,\theta_{\mathbf{q}}^2}\right). \tag{35}$$

Equation (35) yields $\theta_g=15.6°$, in agreement with the experiment. Note that $\theta_g$ is 4.1° further out from the $c$ axis than $\theta_{\mathbf{q}}=11.5°$ pertaining to the relevant $\omega$ and $\Delta\alpha$, signifying defocusing. In terms of the focusing parameter, the disparity between $\theta_g$ and $\theta_{\mathbf{q}}$ corresponds to $p=+0.18\pm0.02$, in accord with $p=+0.176$ derived from Eq. (21).

## V. CONCLUDING REMARKS

Coherent longitudinally polarized acoustic beams of gigahertz frequencies have been generated in a solid medium ($PbMoO_4$) by the use of periodic laser-induced heating of a thin metallic transducer. The mechanism of generation is essentially based on the strain provided by thermoelastic expansion synchronous with the optical difference frequency, in accordance with the observed acoustic resonances within the transducer and the quadratic dependence of the acoustic intensity on the laser power, as well as the overall intensity. An obvious advantage of the method is the simple tuning of the acoustic frequency via the difference frequency of the interfering lasers. The method is furthermore applicable at cryogenic temperatures, despite the decline of thermal expansion.

For the detection we have relied on Brillouin scattering, which, however, is limited to frequencies up to, say, 15 GHz. The generation mechanism, on the other hand, seems limited by electron-phonon relaxation to several hundreds of gigahertz, easily accessible by light modulation through interference.[36] The usage of other phonon detection techniques, such as bolometers or superconducting tunnel junctions,[37–39] could therefore markedly extend the useful frequency range.

We have further investigated some aspects related to the propagation of the acoustic beam, in particular its divergence by diffraction, which appears governed by Fresnel diffraction provided phonon focusing is taken into account. In the Fraunhofer regime, the effects are to increase the divergence by a factor $1/(1-2p)$.

By virtue of its monochromaticity and directionality the generated phonon beam is particularly suited to measure phonon decay versus the frequency. The beam further is responsive to the phase distribution of the laser heating over the focal area. This allows one to manipulate the beam in various ways, such as by simulating acoustic lens just below the emitting ''orifice'' or sweeping the beam by a sideward moving grating. Combined with Brillouin detection, which distinguishes between phase and group velocities, the latter option allows a direct measurement of phonon focusing. We finally note from further analysis of Fig. 10 that the acoustic divergence seems to slightly increase upon going away from the high-symmetry $c$ axis, in keeping with the arguments by Maris.[40]

## ACKNOWLEDGMENTS

The authors wish to thank Femius Koenderink, Han-Kwang Nienhuys, and Mark de Vries for valuable help. The work was supported by the Netherlands Foundation ''Fundamenteel Onderzoek der Materie (FOM)'' and the ''Nederlandse Organisatie voor Wetenschappelijk Onderzoek (NWO).''

[1] R. M. White, J. Appl. Phys. **34**, 3559 (1963).
[2] R. J. von Gutfeld and A. H. Nethercot, Phys. Rev. Lett. **12**, 641 (1964); R. J. von Gutfeld and R. L. Melcher, Appl. Phys. Lett. **30**, 257 (1977).
[3] W. Eisenmenger and A. H. Dayem, Phys. Rev. Lett. **18**, 125 (1967); W. Eisenmenger, in *Physical Acoustics*, edited by W. P. Mason (Academic Press, New York, 1976), Vol. 12, p. 79.
[4] H. Kinder, Phys. Rev. Lett. **28**, 1564 (1972); P. Berberich, R. Buemann, and H. Kinder, *ibid.* **49**, 1500 (1982); G. P. Scherg, R. Gärtner, P. Berberich, and H. Kinder, in *Proceedings of the Seventh International Conference on Phonon Scattering in Condensed Matter*, edited by M. Meissner and R. O. Pohl (Springer-Verlag, Berlin, 1992), p. 266.
[5] K. F. Renk, in *Nonequilibrium Phonons in Nonmetallic Crystals*, edited by W. Eisenmenger and A. A. Kaplyanskii (North-Holland, Amsterdam, 1986), p. 277; K. F. Renk, *ibid.*, p. 317.
[6] C. Thomsen, H. T. Grahn, H. J. Maris, and J. Tauc, Phys. Rev. B **34**, 4129 (1986).
[7] E. P. N. Damen, A. F. M. Arts, and H. W. de Wijn, Phys. Rev. Lett. **74**, 4249 (1995).
[8] B. Taylor, H. J. Maris, and C. Elbaum, Phys. Rev. B **3**, 1462 (1971).
[9] F. Rösch and O. Weis, Z. Phys. B **25**, 101 (1976); **25**, 11 (1976).
[10] A. G. Every, Phys. Rev. B **24**, 3456 (1981); **34**, 2852 (1986).
[11] E. Hartley and S. Wagner, Rev. Sci. Instrum. **62**, 321 (1991).
[12] Isomet Corporation (private communication).
[13] J. R. Sandercock, in *Light Scattering in Solids III*, Topics in Applied Physics, Vol. 51, edited by M. Cardona and G. Güntherodt (Springer-Verlag, Berlin, 1982), Chap. 6.
[14] G. L. Eesly, Phys. Rev. B **33**, 2144 (1986); Phys. Rev. Lett. **58**, 1680 (1987).
[15] Y. A. Touloukian *et al.*, *Thermophysical Properties of Matter* (IFI/Plenum, New York, 1970), Vols. 1, 4, 10, and 12.
[16] G. A. Coquin, D. A. Pinnow, and A. W. Warner, J. Appl. Phys. **42**, 2162 (1971).
[17] H. S. Carslaw and J. C. Jaeger, *Conduction of Heat in Solids*, 2nd ed. (Oxford University Press, Oxford, 1959).
[18] G. Cachier, J. Acoust. Soc. Am. **49**, 974 (1971).
[19] J. M. Ziman, *Electrons and Phonons* (Oxford University Press, Oxford, 1960).
[20] H. M. Rosenberg, *Low Temperature Solid State Physics* (Oxford University Press, Oxford, 1963).
[21] E. P. N. Damen, A. F. M. Arts, and H. W. de Wijn, Phys. Rev. B **59**, 349 (1999).
[22] M. Born and E. Wolf, *Principles of Optics*, 6th ed. (Pergamon Press, 1980).
[23] H. Kogelnik and T. Li, Proc. IEEE **54**, 1312 (1966).
[24] W. Demtröder, *Laser Spectroscopy*, 2nd ed. (Springer-Verlag, Berlin, 1996), p. 363.
[25] A. Papoulis, *Systems and Transforms with Applications in Optics* (McGraw-Hill, New York, 1968).
[26] J. P. Wolfe, *Imaging Phonons* (Cambridge University Press, Cambridge, England, 1998).
[27] G. A. Northrop and J. P. Wolfe, Phys. Rev. B **22**, 6196 (1980); D. C. Hurley and J. P. Wolfe, *ibid.* **32**, 2568 (1985); S. E. Hebboul and J. P. Wolfe, Z. Phys. B: Condens. Matter **74**, 35 (1989).
[28] M. R. Hauser, R. L. Weaver, and J. P. Wolfe, Phys. Rev. Lett. **68**, 2604 (1992).
[29] E. Held, W. Klein, and R. P. Huebener, Z. Phys. B: Condens. Matter **75**, 17 (1989).
[30] J. F. Nye, *Physical Properties of Crystals* (Oxford University Press, Oxford, 1985).
[31] H. J. Maris, in *Nonequilibrium Phonons in Nonmetallic Crystals*, edited by W. Eisenmenger and A. A. Kaplyanskii (North-Holland, Amsterdam, 1986), p. 51.
[32] J. M. Farley, G. A. Saunders, and D. Y. Chung, J. Phys. C **8**, 780 (1975).
[33] S. A. Self, Appl. Opt. **22**, 659 (1983).
[34] C. Herring, Phys. Rev. **95**, 954 (1954).
[35] D. J. Dieleman, A. F. Koenderink, A. F. M. Arts, and H. W. de Wijn, Phys. Rev. B **60**, 14 719 (1999).
[36] R. E. Drullinger, K. M. Evenson, D. A. Jennings, F. R. Petersen, J. C. Bergquist, Lee Burkings, and H.-U. Daniel, Appl. Phys. Lett. **42**, 137 (1983).
[37] T. Ishiguro and S. Morita, Appl. Phys. Lett. **25**, 533 (1974).
[38] C. Boragno, U. Valbusa, and G. Pignatel, Appl. Phys. Lett. **50**, 583 (1987).
[39] N. E. Booth, Appl. Phys. Lett. **50**, 293 (1987).
[40] H. J. Maris, Phys. Rev. B **28**, 7033 (1983).